energies

MDPI

Article

Experimental Investigation of Pore Characteristics and Permeability in Coal-Measure Sandstones in Jixi Basin, China

Huazhou Huang [1,2,3,*], Yuantao Sun [2,3], Xiantong Chang [2,3], Zhengqing Wu [2,3], Mi Li [2,3] and Shulei Qu [2,3]

[1] Jiangsu Key Laboratory of Coal-Based Greenhouse Gas Control and Utilization, China University of Mining and Technology, Xuzhou 221008, China
[2] Key Laboratory of Coalbed Methane Resources and Reservoir Formation Process, China University of Mining and Technology, Ministry of Education, Xuzhou 221008, China
[3] School of Resources and Geosciences, China University of Mining and Technology, Xuzhou 221008, China
* Correspondence: huazhouh@163.com

Abstract: The research of pore and permeability characteristics of tight sandstone reservoirs in coal-measure is critical for coal-measure gas development. In this study, the pore systems of tight sandstones were studied based on low-field nuclear magnetic resonance (LF-NMR) data. The permeability of tight sandstones was obtained by the tester based on the pulse transient method. The permeability variation with the effective stress, grains, and pore characteristics was analyzed. The results show that the tight sandstone reservoirs in the coal-measure have low total porosity (2.80–4.14%), low effective porosity (0.51–1.56%), and low permeability (0.351×10^{-6}–13.910×10^{-6} um^2). LF-NMR T_2 spectra of the testing sandstones show that the micropores are the most developed, but most of the micropores are immovable pores. The pore characteristics are significantly affected by the grain size of sandstones. The pore connectivity ranks from good to poor with decreasing sandstone particle size. The total porosity and effective porosity increase with the grain size. There is a near-linear negative relationship between permeability and effective stress when the effective stress is between 405 psi and 808 psi. The greater the number of movable pores and the larger the effective porosity, the bigger the permeability of the sandstone. The effective porosity of sandstones is a sensitive indicator for evaluating the permeability of tight sandstone reservoirs. The stress sensitivity coefficient of permeability (S_s) increases with the increase of the effective stress. The sandstone with lower permeability, smaller effective porosity, and finer grains has a higher S_s. The particle size of sandstone from coal-measure has a great influence on both permeability and S_s. The findings will provide a better understanding of the characterization of pore structure and permeability in the process the coal-measure gas extraction, which is useful for the efficient development of coal-measure gas.

Keywords: sandstone; permeability; pore characteristics; permeability stress sensitivity; Jixi Basin

Citation: Huang, H.; Sun, Y.; Chang, X.; Wu, Z.; Li, M.; Qu, S. Experimental Investigation of Pore Characteristics and Permeability in Coal-Measure Sandstones in Jixi Basin, China. *Energies* **2022**, *15*, 5898. https://doi.org/10.3390/en15165898

Academic Editor: Rouhi Farajzadeh

Received: 14 July 2022
Accepted: 11 August 2022
Published: 14 August 2022

1. Introduction

The coal-measure formation is rich in unconventional natural gas resources, which is called coal-measure gas, including coalbed methane in coal reservoirs, tight sandstone gas in sandstone reservoirs, and shale gas in shale reservoirs [1,2]. Coal-measure gas development has attracted global attention because of its huge resource potential, especially in China [1,3,4]. Coal seams are generally mixed with sandstones, mudstones, and shales in coal-measure [5]. Coal seams and shale in the coal-measure could be the main source rocks for coal-measure gas because they are favorable for hydrocarbon generation and gas accumulation, while the conditions, such as burial depth, time, and temperature, are appropriate [1,6,7]. Sandstones in the coal-measure are one kind of reservoir that could store gas charged by the above source rocks [4,6,8,9]. Most of the sandstones in coal-measure are tight sandstones because their porosity is less than 10%, and their permeability is less than 0.1 mD [1,6,10]. The reservoir characteristics among the coal, shale, and sandstone in the coal-measure vary greatly [11]. The pore and permeability characteristics of the

coal-measure gas reservoir could affect the gas accumulation and production [12,13]. Many studies have focused on the reservoir characteristics of coal [14,15], while the research on the pore and permeability characteristics of tight sandstone in coal-measure in the study area has been less focused upon. The tight sandstones in coal-measure are characterized by smaller pores and complex pore throat connections [16], which lead to lower permeability. The research on pore and permeability characteristics of tight sandstone reservoirs is critical for coal-measure gas development [15].

Low field nuclear magnetic resonance (LF-NMR) is a non-destructive method to characterize the pore structure parameters of complex porous media on a wide scale compared with N_2 adsorption and mercury porosimetry [1,4,17–19]. The sandstone sample should be saturated with water when the pore characteristics of the sandstone are obtained by LF-NMR. The water-saturated sample is then placed in a strong static magnetic field generated by an external magnet, and a small radio frequency magnetic field is superimposed on the static magnetic field to excite the hydrogen nuclei in the water, thereby inducing nuclear magnetic resonance [20]. When the radio frequency field is turned off, a signal varying with time can be received [21]. The amplitude of the signal change can be described by the longitudinal relaxation time (T_1) and the transverse relaxation time (T2). For LF-NMR, T_2 carries similar information to that of T_1 [20,22,23]. Therefore, T_2 is generally applied to the analysis of the pore structure parameters of sandstone samples. Pore sizes, porosity, pore connectivity, and pore throat distribution for tight sandstone reservoirs could be characterized by the relaxation time T_2 distribution [1,14,19,24]. However, it cannot determine the permeability of the sandstone directly [1,16]. Tight sandstone reservoirs have complex, highly heterogeneous pore structures, and poor pore connectivity [1,25]. The pore size and pore distribution vary greatly for the samples with different lithology. There is a close relationship between permeability and pore characteristics including porosity, pore-throat size, and pore volume [14,15,26,27]. The permeability of tight sandstones cannot be assessed only by total porosity because of the sandstone's complex pore-throat geometry [26,28]. However, the movable fluid porosity attained by LF-NMR might have a certain indication on permeability [1,14].

The previous reports have studied the relationship between permeability and scaling in the water injection, pore fluid pressure, confining pressure, and effective stress [29–32]. Generally, permeability decreases with the rise of the confining pressure and the effective stress [31], the permeability declines dramatically under 4–8 MPa confining stress, and permeability reduces slightly for 8–12 MPa conditions [29–31]. In a deep coal-measure reservoir, stress increases with the burial depth, which results in low permeability. The extraction of coal-measure gas would increase the effective stress on pores and fractures, which results in the compression of pores and the closure of fractures [29,31,33–37]. The permeability of the reservoir gradually decreases with the increase of the effective stress in the process of coal-measure gas extraction [38]. This kind of phenomenon is known as the stress sensitivity of the reservoir [39]. The permeability loss by the stress sensitivity will significantly affect the water and gas production rate because the original permeability of the coal-measure reservoir is generally low [15,29,38,40,41]. The stress sensitivity coefficient of reservoir permeability (S_s) for sandstones [37,42] is an index of reservoir permeability in response to effective stress variation [38], which could be affected by the plastic mineral content, pore throat size, porosity, permeability, etc. [37]. For instance, a higher the plastic mineral content could result in a bigger S_s [37].

The effect of sandstone grains on pore characteristics, permeability, and S_s is still unclear, and the relevant research about that is of great significance to coal-measure gas production [26,37,38,43,44]. The objective of this study was to analyze the characteristics of pore systems and permeability in tight sandstones with different grains based on Coal-measure Gas Well HJD1 in Jixi Basin in Northeast China. The pore systems were studied based on LF-NMR data. The permeability was obtained by the tester based on the pulse transient method. The effects of pore characteristics on permeability variation were discussed. Then, permeability variation with effective stress and grain size of sandstones were

analyzed in detail. The findings will provide a better understanding of the characterization of pore structure and permeability in the process of coal-measure gas extraction, and will be useful for the efficient development of coal-measure gas.

2. Geological Setting

Jixi Basin is mainly composed of the northern depression and the southern depression, which are separated by the central Mashan fault (Figure 1a). Large-angle normal faults are well developed in the basin. The strikes of the faults are mainly east–west and northeast.

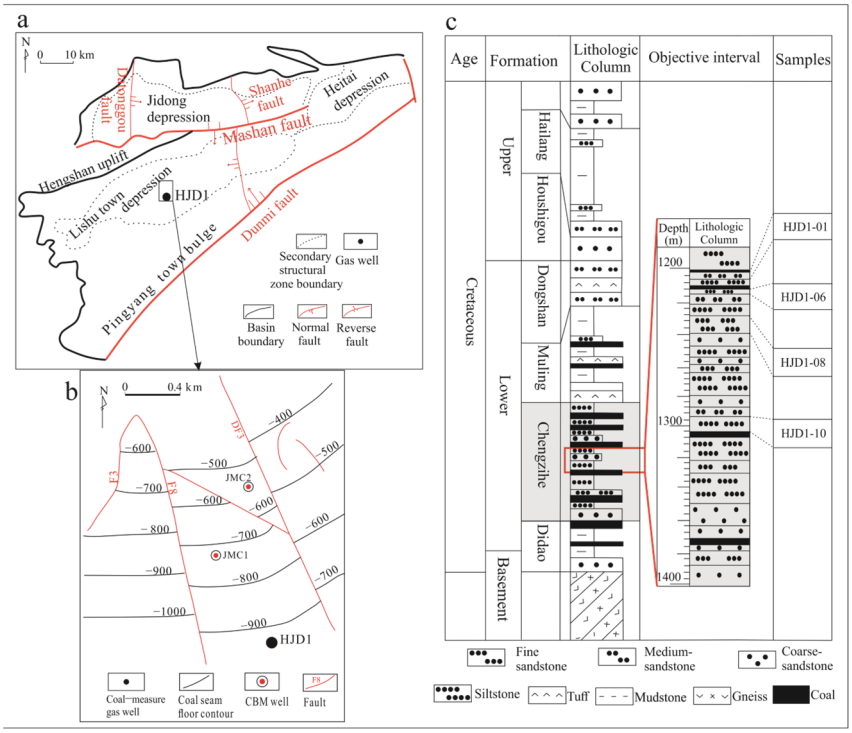

Figure 1. Geological background of the study area: (**a**) Location of Coal-measure Gas Well HJD1 in Jixi Basin; (**b**) geological structure of the area where Well HJD1 is located; (**c**) sampling stratigraphic column in Well HJD1.

The Quaternary in the Cenozoic and the Lower Cretaceous in the Mesozoic are the main strata in the research area where Well HJD1 is located (Figure 1). The Lower Cretaceous covers the Jixi Group and Huashan Group. The Jixi Group consists of Didao Formation, Chengzihe Formation, and Muling Formation from bottom to top (Figure 1c). The Muling Formation and Chengzihe Formation in the Lower Cretaceous are the main coal-bearing strata. Well HJD1 was constructed for coal-measure gas extraction from the Chengzihe Formation in the Jixi Basin, which is in eastern Heilongjiang province, in northeast China.

The Chengzihe Formation is the target strata in this research (Figure 1c). The buried depth of the Chengzihe Formation in Well HJD1 is 767.50–1739.05 m. The Chengzihe Formation is mainly composed of siltstone, fine sandstone, and coal seam. The sandstone samples used in this study are taken from the middle section of the Chengzihe Formation. The main coal seams involved in the sampling section are Numbers 22, 23, 25, and 28, respectively. In addition, most sandstone layers are between 2–8 m in thickness, as the sandstone layers are separated by thin mudstone layers and coal seams. The grains of sandstone also vary greatly.

3. Samples and Experimental Methods

3.1. Sample Collection and Processing

There are 4 sandstone samples collected from Well HJD1: medium sandstone (HJD1-01), fine sandstone (HJD1-06 and HJD1-08), and siltstone (HJD1-10). The 4 sandstone samples were lithologically classified according to the rock flake identification standard SY/T5368-2016 issued by the National Energy Administration in China. The grain size, and the percentage of clastic constituents and clay of the four samples can be seen in Table 1. The appearance of the rock samples was gray white sandstone without visible cracks.

Table 1. Rock thin section identification results of sandstone samples.

Sample No.	Clastic Constituents/%				Matrix/%	Grain Size/mm	Lithology
	Quartz	Feldspar	Detritus	Mica	Clay		
HJD1-01	56	12	13	3	-	0.30–0.50	Medium sandstone
HJD1-06	32	28	13	2	23	0.05–0.10	Fine sandstone
HJD1-08	55	18	11	1	10	0.06–0.12	Fine sandstone
HJD1-10	15	11	-	-	72	0.03–0.06	Siltstone

The collected sandstones were made into cylinders for permeability testing with a diameter of 50 mm and a height of 30 mm–100 mm. In addition, the flatness of the top and bottom surfaces of the sandstone samples was within 0.05 mm. Then, these samples were washed and dried before the test, in accordance with the requirements of Practices for Core Analysis (SY/T5336-2006).

HJD1-10 (silts sandstone), HJD1-06 (fine sandstone), and HJD1-01 (medium sandstone) are sandstones with different grain sizes. They were selected to undergo LF-NMR experiments. The LF-NMR experiments were conducted to characterize the pore system of the sampling sandstones and illustrate the effect of pore characteristics on the permeability of the sandstone.

3.2. Permeability Experiment

The permeability was tested by a Pulse Decay Permeameter-PDP-200 (American Core Lab Company, Tulsa, OK, USA, Figure 2), which was based on the pulse transient method. The permeability could be obtained based on the pressure decay curve. Practices for Core Analysis (SY/T5336-2006) was the reference method for this experiment, and the test gas was nitrogen. Permeability experiments were conducted by increasing the confining pressure and fixed pore pressure. This simulates the increasing effective stress during the coal-measure gas development.

Figure 2. Pulse Decay Permeameter-PDP-200.

In this experiment, the test sample was put into a closed container, then the initial pressure was set, and time allowed for the initial pressure to reach the equilibrium state. Then, a pulse pressure (ΔP) was applied to the top of the sample. The gas percolated through the sample under the pressure ΔP, and this process resulted in the decrease of the pressure of the top container and the increase of the pressure of the bottom container. Finally, another equilibrium state (P_f) was reached between the top container and the bottom container; there was no pressure difference attenuation.

The intake nitrogen gas pressure, which is also known as pore pressure, was set to 700 psi, and the average pore pressure stabilized between 682 psi and 704 psi. The confining pressure for each sample was set to 1100 psi, 1200 psi, 1300 psi, 1400 psi, and 1500 psi to obtain the permeability. The temperature in the permeability tests was the indoor atmospheric temperature (about 25 °C).

3.3. LF-NMR Experiments

The LF-NMR experiments were performed by the MesoMR23-060H-I instrument with a main frequency of 23.400 MHz (Figure 3). The temperature of the laboratory where the NMR experiments were performed was 23.5 °C, the magnet temperature was constant at (35 ± 0.02) °C, the echo spacing was 0.1 ms, the numbers of scans were 32, and the echo numbers were 8000.

Figure 3. MesoMR23-060H-I instrument for LF-NMR experiments.

First, the columnar sandstone samples were dried. The sample was put into a 101 electric heating blast box for nearly 24 h until its weight remained constant. In addition, the samples were vacuumed for 2 h, and then they were saturated with water for nearly 24 h in the 2XZ-4B vacuum-saturation device. The quality difference of the sandstone sample before and after saturation was less than 0.05%. Moreover, the T_2 spectrum distribution of the saturated sandstone sample was obtained by the NMR test instrument. After that, the movable water within the saturated sandstone sample was removed by the TCL-21M desktop high-speed refrigerated centrifuge. Finally, the T_2 spectrum distribution of the centrifuged sandstone samples was tested by the MesoMR23-060H-I instrument.

In an LF-NMR test, the number of hydrogen atoms present within a fluid in a porous medium can be detected by the transverse relaxation time (T_2) [1,14], and the T_2 spectrum is generally used to characterize the physical parameters of the rock, such as pore size distribution and connectivity. It is supposed that longer T_2 corresponds to larger pores, while shorter T_2 corresponds to the smaller pores [4,28]. The amplitude of the T_2 distribution reflects the number of pores within a certain size. The higher the amplitude, the greater the number of pores [20,21].

The application of NMR in the study of pore types in sandstone is based on the fact that T_2 is positively correlated with pore size. This relationship can be expressed as [20,28,45]:

$$\frac{1}{T_2} = \rho_2\left(\frac{S}{V}\right) \quad (1)$$

where T_2 is the transverse relaxation time resulted from surface interactions, ms; and ρ_2 is a constant representing the transverse relaxation strength, μm/ms; S is the surface area of pores (cm^2); and V is the pore volume (cm^3).

4. Results

4.1. Permeability

The permeability of testing sandstones was between 0.351×10^{-3}–13.910×10^{-3} mD under the confining pressure of 1100–1500 psi. The permeability of the medium sandstone was the highest, followed by the fine sandstone, and the siltstone was the smallest under similar pore pressure and confining pressure.

For the medium sandstone (HJD1-01), its permeability was between 11.160×10^{-4}–13.910×10^{-3} mD under the confining pressure of 1100–1500 psi, with an average of 10.118×10^{-3} mD (Table 2).

Table 2. Permeability results.

Sample Number	Test Gas	Confining Pressure/psi	Average Pore Pressure/psi	Permeability/ $\times 10^{-3}$ mD	Lithology	Sampling Depth/m
HJD1-01	N_2	1100	695	13.910	Medium sandstone	1201.60–1201.88
	N_2	1200	700	13.410		
	N_2	1300	699	12.860		
	N_2	1400	704	12.110		
	N_2	1500	704	11.160		
HJD1-06	N_2	1100	687	1.188	Fine sandstone	1300.12–1300.54
	N_2	1200	695	1.081		
	N_2	1300	697	0.891		
	N_2	1400	697	0.738		
	N_2	1500	703	0.689		
HJD1-08	N_2	1100	691	1.060	Fine sandstone	1301.88–1302.5
	N_2	1200	700	0.932		
	N_2	1300	705	0.788		
	N_2	1400	705	0.656		
	N_2	1500	704	0.594		
HJD1-10	N_2	1100	693	0.643	Siltstone	1380.95–1381.82
	N_2	1200	707	0.571		
	N_2	1300	682	0.489		
	N_2	1400	698	0.410		
	N_2	1500	699	0.351		

For the fine sandstone (HJD1-06, HJD1-08), the permeability was between 0.594×10^{-3}–1.188×10^{-3} mD. The permeability of HJD1-06 was between 1.188×10^{-3}–0.689×10^{-3} mD and the average permeability was 0.917×10^{-3} mD under 1100–1500 psi confining pressure. The permeability of HJD1-08 between 1.060×10^{-3}–0.594×10^{-3} mD and the average value was 0.806×10^{-3} mD under the condition of 1100–1500 psi confining pressure (Table 2).

For the siltstone (HJD1-10), its permeability was between 0.351×10^{-3}–0.643×10^{-3} mD, with an average of 0.493×10^{-3} mD (Table 2).

The grain size of sandstone has an obvious effect on permeability. The permeability of the sampling sandstone increases with the increase of grain size. The permeability of the medium sandstone (HJD1-01) with an average of 10.118×10^{-3} mD was higher than that of the other samples. However, the permeability of the fine sandstone (HJD1-06 and HJD1-08)

and the siltstone (HJD1-10) was relatively close. The permeability of the fine sandstone was bigger than that of the siltstone under similar confining pressure and pore pressure.

The permeability and confining pressure are negatively correlated. The permeability gradually decreases as the confining pressure increases for the medium sandstone, the fine sandstone, and the siltstone (Figure 4). The decrease in permeability for HJD1-01, HJD1-06, HJD1-08, and HJD1-10 while the confining pressure increased from 1100 to 1500 psi was 2.75×10^{-3} mD, 0.499×10^{-3} mD, 0.466×10^{-3} mD, and 0.292×10^{-3} mD, respectively.

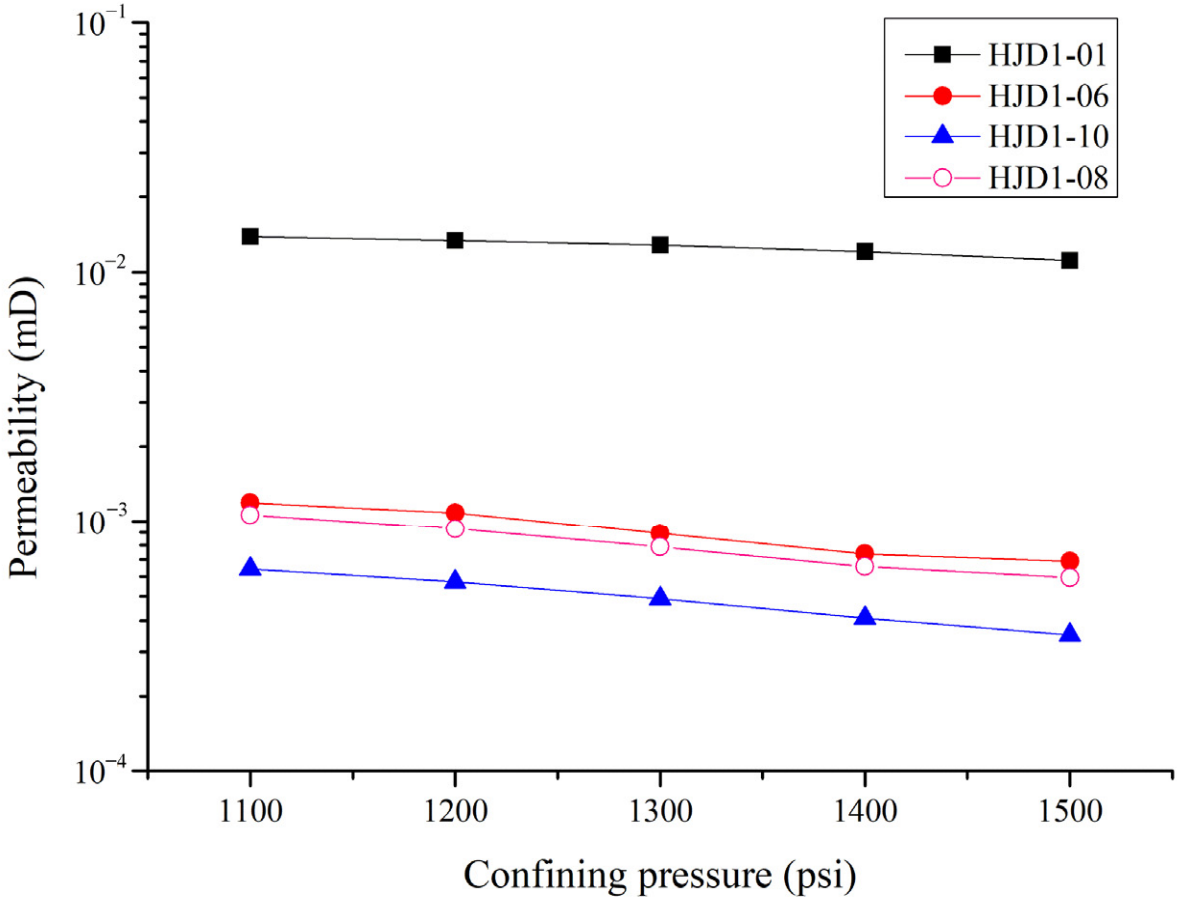

Figure 4. Relationship between confining pressure and permeability.

4.2. LF-NMR Pore Characteristics

The pore size distribution, total porosity, effective porosity, and the T_{2C} value could be obtained by the T_2 spectrum [1,14,46]. The T_2 spectra of the sampling sandstones under the water-saturated condition and the centrifugal condition is shown in Figure 5a–c. T_2 spectra for three sandstones range from 0.01 to 1889.65 ms. T_2 spectra of HJD1-01, HJD1-06, and HJD1-10 show a wide bimodal distribution with a main peak and a subpeak. There is a significant difference in T_2 distribution between the three sandstones (Figure 5d). The main peak of HJD10 is separate from the subpeak; however, the main peak of HJD1-01 and HJD1-06 is interconnected with the subpeak. The main peaks of HJD1-01, HJD1-06, and HJD1-10 are within 0.13–11.09 ms, 0.13–9.66 ms, and 0.01–1.38 ms. The subpeaks of HJD1-01, HJD1-06, and HJD1-010 are within 11.09–1889.65 ms, 9.66–666.99 ms, and 12.75–622.25 ms.

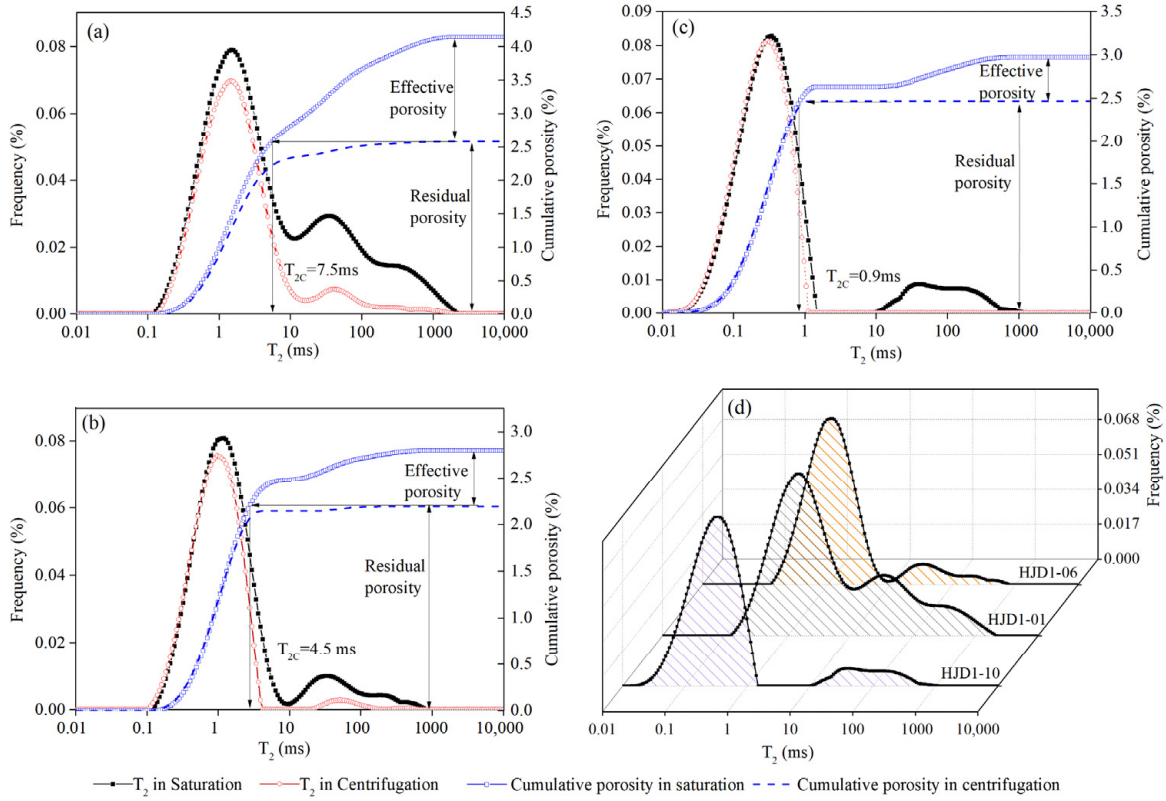

Figure 5. T_2 spectra showing the porosity of different sampling sandstones: (**a**) NMR measurements of HJD1-01 under the water-saturated condition and centrifugal condition; (**b**) NMR measurements of HJD1-06 under the water-saturated condition and centrifugal condition; (**c**) NMR measurements of HJD1-10 under the water-saturated condition and centrifugal condition; (**d**) contrast of T_2 spectra under the water-saturated condition between HJD1-01, HJD1-06, and HJD1-10.

T_2 distribution is closely related to the size of the pores. Generally, the longer T_2, the bigger the pore size. In contrast, the shorter T_2, the smaller the pore size. The characteristics of the pores in sandstone could be analyzed by the distribution position and the area of the T_2 spectrum [14]. The area of the peaks reflects the number of pores within a certain size; the larger the area, the greater the number of pores. The peak width suggests the distribution of a certain kind of pore, while the number of peaks reflects the continuity of pores at all levels. The two peaks of the T_2 spectra reflect the two main types of pores. Based on the T_2 spectra curve of HJD1-01, HJD1-06, and HJD1-10, micropores correspond to $T_2 < 11.09$ ms, and macropores correspond to 11.09 ms $< T_2 <$ 1889.65 ms. The micropores peak of the T_2 spectra is the largest, indicating that the micropores are the most developed. The bigger the value of T_2, the bigger the pore size of the sandstone. The pore size of the micropores from big to small is HJD1-01, HJD1-06, and HJD1-10, The pore size of the macropores from big to small is HJD1-01, HJD1-06, and HJD1-10 as well.

The T_2 spectrum morphology of the peak in the saturated state is very close to that after centrifugation (Figure 5c). This means the residual water trapped in the pores cannot be removed by centrifugation, which indicates that the connectivity of the pores is poor. Otherwise, the T_2 spectrum morphology of the peak after centrifugation is very different from the peak in the saturated state; this indicates that the connectivity of pores is good, and the pores are very conducive to gas flow. According to Figure 5a–c, the macropore connectivity in the three testing samples is relatively good, which is significantly better than that of the micropores. Furthermore, there are obvious differences in the connectivity of micropores among the three sandstone samples; the micropores' connectivity is in the order from good to poor: HJD1-01, HJD1-06, HJD1-10.

The connection between the main peak and the subpeak could be used to identify the connectivity among pores [14]. For instance, there is a gap between the main peak and subpeak in the siltstone (HJD1-10) in Figure 5c, meaning the connection between micropores and macropores is poor. In contrast, the main peak is interconnected with the subpeak in HJD1-01 (Figure 5a) and HJD1-06 (Figure 5b), which suggests the pore connectivity of HJD1-01 and HJD1-06 is better than that of HJD1-10 between micropores and macropores. In general, the pores in the siltstone (HJD1-10) had poorer pore connectivity than that of the medium stone and the fine stone (HJD1-01, HJD1-06) [47].

The distribution position and area of the T_2 spectrum of medium sandstone, fine sandstone, and siltstone are different [47], which suggests that sandstone grains can affect pore characteristics. For example, the distribution area of T_2 spectra representing macropores in HJD1-1 (Figure 5a) is much larger than that of HJD1-6 and HJD1-10 (Figure 5b,c).

The porosity of sandstones can be analyzed based on LF-NMR T_2 [14,48]. Total porosity in the saturated state and centrifugal state can be obtained by separate NMR tests (Figure 5a–c). The maximum value of the cumulative porosity in the saturated water state is known as the total porosity [14,49]. There is residual water in the sample after centrifugation. The maximum value of the cumulative porosity after centrifugation could be seen as the residual porosity. The difference between the total porosity and the residual porosity is the porosity occupied by free water, which can be regarded as the effective porosity. The total porosity of HJD1-01, HJD1-06, and HJD1-10 was 4.14%, 2.80%, and 2.97%. The effective porosity of HJD1-01, HJD1-06, and HJD1-10 was 1.56%, 0.60%, and 0.51%. The proportion of the effective porosity to the total porosity for HJD1-01, HJD1-06, and HJD1-10 was 37.68%, 21.42%, and 17.18% (Table 3).

Table 3. Results of NMR analysis.

Sample	T_{2C}	Total Porosity	Residual Water Porosity	Effective Porosity	Pore Proportion (%)		
ID	(ms)	(%)	(%)	(%)	$T_2 < T_{2C}$	$T_2 > T_{2C}$	Effective Porosity/Total Porosity
HJD1-01	5.54	4.14	2.58	1.56	61.50	38.50	37.68
HJD1-06	2.77	2.80	2.20	0.60	79.07	20.93	21.42
HJD1-10	0.85	2.97	2.46	0.51	81.95	18.05	17.17

The T_{2C} value can be obtained by the following steps. First, draw a line parallel to the *X*-axis with the residual porosity (Figure 5a–c). This parallel line has an intersection point with the saturated cumulative porosity curve. The X value corresponding to this intersection point is T_{2C} [14,50]. T_{2C} can divide the T_2 spectrum into two segments: one segment corresponds to pores with water that could not be drained, and the other segment corresponds to pores with water that could be drained. Pores with water that could not be drained are known as immovable pores, pores with water that could be drained are called movable pores. Therefore, the pore size at the T_{2C} value is taken for the separation between the immovable pore volume and the movable pore volume [14]. The T_2 spectrum which is less than T_{2C} corresponds to micropores with poorer pore connectivity, which are the immovable pores. The T_2 spectrum which is bigger than T_{2C} corresponds to macropores with better pore connectivity which are the movable pores [15]. T_{2C} was 5.54 ms, 2.77 ms, and 0.85 ms for HJD1-01, HJD1-06, and HJD1-10, respectively. Almost all of the micropores were immovable pores in the three samples. The proportion of immovable pores to total pores for HJD1-01, HJD1-06, and HJD1-10 was 61.50%, 79.07%, and 81.95%, respectively. The proportion of movable pores to total pores for HJD1-01, HJD1-06, and HJD1-10 was 38.50%, 20.93%, and 18.05% (Table 3).

5. Discussion

5.1. Permeability Variation with Effective Stress and Grains

The permeability decreases with the increase of the effective stress; the relationship between the permeability and the effective stress is close to the linear relation when the effective stress is between 405 psi and 808 psi because the R^2 of all the samples is more than 0.9757 (Table 4, Figure 6).

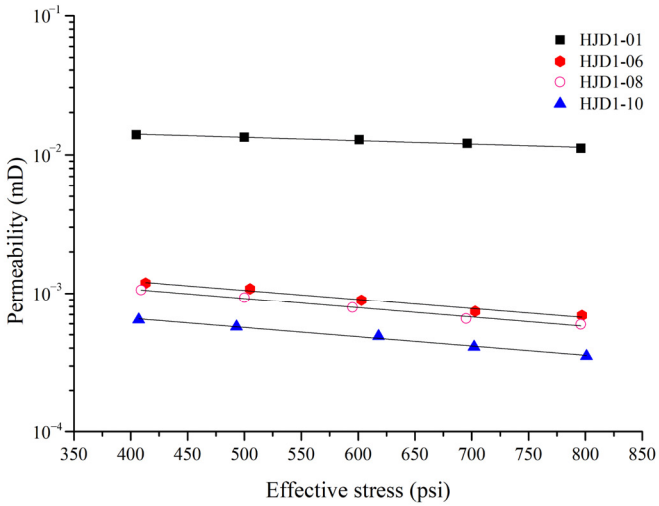

Figure 6. Relationship between the effective stress and permeability.

Table 4. Linear fitting results between permeability (y, mD) and effective stress (x, psi).

Sample	Fitting Liner Equations	R^2
HJD1-01	$y = -6.95 \times 10^{-6}x + 16.86 \times 10^{-3}$	0.9757
HJD1-06	$y = -1.39 \times 10^{-6}x + 1.76 \times 10^{-3}$	1
HJD1-08	$y = -1.24 \times 10^{-6}x + 1.55 \times 10^{-3}$	1
HJD1-10	$y = -0.75 \times 10^{-6}x + 0.94 \times 10^{-3}$	1

The grain size of sandstone has a significant impact on sandstone permeability [51]. The permeability decreases in the order of medium sandstone, fine sandstone, and siltstone under similar effective stress. For the medium sandstone (HJD1-01), the fine sandstone (HJD1-06), and the siltstone (HJD1-10), the slope in Figure 6 is -6.95×10^{-6}, -1.39×10^{-6}, and -0.75×10^{-6}, respectively, as the effective stress increases from nearly 400 psi to 800 psi.

The rock permeability damage by the stress sensitivity could be expressed by the permeability stress sensitivity coefficient. The greater the stress sensitivity coefficient, the better the stress sensitivity will be. The calculation formula is as follows [38]:

$$S_S = \frac{\left[1 - \sqrt[3]{\frac{K_i}{K_0}}\right]}{\log_{10} \frac{\delta_i}{\delta_0}} \quad (2)$$

where S_S is the permeability stress sensitivity coefficient, dimensionless; K_i is the permeability of the sample under δ_i, mD; K_0 is the permeability under δ_0, mD; δ_i is the effective stress at any time, psi; and δ_0 is the initial effective stress, psi.

Generally, S_s would increase for the same sample with the increase of the effective stress (Table 5). It seems that the sample with lower permeability and finer grains has a higher S_S. The permeability of the medium sandstone (HJD1-01) is much higher than that of the other samples (including HJD1-06 and HJD1-08) with similar initial effective stress, and the S_s of HJD1–01 is much lower than the other samples with similar effective stress. For the

fine sandstone samples HJD1-06 and HJD1-08, the higher the permeability, the lower the stress sensitivity. This agrees with the reports that sandstones with very low permeability are affected by stress to a greater degree than those with higher permeability [52,53]. S_S could be affected by the sandstone grains. The S_s of the medium sandstone is a bit lower than that of the fine sandstone and the siltstone. However, the S_s of the fine sandstone and the siltstone is relatively close (Table 5).

Table 5. Stress sensitivity coefficient (S_S) under different effective stress between 405 and 801 psi.

Sample Number	Lithology	Effective Stress/psi	Permeability/ $\times 10^{-3}$ mD	S_S
HJD1-01	Medium sandstone	405	13.91	-
		500	13.41	0.1325
		601	12.86	0.1506
		696	12.11	0.1920
		796	11.16	0.2412
HJD1-06	Fine sandstone	413	1.188	-
		505	1.081	0.3546
		603	0.891	0.5563
		703	0.738	0.6352
		797	0.689	0.5816
HJD1-08	Fine sandstone	409	1.06	-
		500	0.932	0.4813
		595	0.788	0.5781
		695	0.656	0.6420
		796	0.594	0.6071
HJD1-10	Siltstone	407	0.643	-
		493	0.571	0.4662
		618	0.489	0.4808
		702	0.41	0.5884
		801	0.351	0.6215

5.2. Effects of NMR Pore Characteristics on Permeability Variation

Generally, the permeability of coal-measure sandstone is controlled by the number of movable pores, effective porosity, and total porosity. The total pore volume from big to small was HJD1-01, HJD1-06, and HJD1-10. The number of micropores and macropores was HJD1-01, HJD1-06, and HJD1-10 in descending order. Almost all of the micropores were the immovable pores in the three samples. The macropore connectivity affects the permeability of the tested samples. Nevertheless, the macropore connectivity in the three testing samples was relatively close. Therefore, the pore volume of the macropores or movable pores was the key factor to the permeability. Large pores are critical to the reservoir quality of the tight sandstone [50]. Movable pores, which are large scale pores with good pore connectivity, dominate the permeability of the reservoir [1,15]. The greater the number of movable pores and the larger the total porosity and the effective porosity, the bigger the permeability of the sandstone. The total porosity of HJD1-01, HJD1-06, and HJD1-10 was 4.14%, 2.80%, and 2.97%. The proportion of movable pores to total pores for HJD1-01, HJD1-06, and HJD1-10 was 38.50%, 20.93%, and 17.17%. The effective porosity of HJD1-01, HJD1-06, and HJD1-10 was 1.56%, 0.60%, and 0.51%. The permeability from big to small was HJD1-01, HJD1-06, and HJD1-10.

Grain size, compaction, and mineral composition could affect the pore structure characteristics [24,37,54]. Finer grain-size sandstones have experienced stronger compaction and cementation during diagenesis in comparison with sandstones with coarser grain size [55]. Stronger compaction and cementation tightly arranged the sandstone's particles and decrease the residual intergranular pores. Therefore, sandstone with a finer grain size develops smaller pore space and a narrower throat [55], which contributes to less total porosity and effective porosity. Mineral composition affects pore-throat structure

parameters such as porosity, pore throat, and effective porosity as well [56]. Sandstones with a coarser grain size have larger rigid grains, such as quartz and feldspar [37]. In the contrary, finer grain-size sandstones have more ductile minerals such as mica and clays [54]. Rigid grains could sustain more pressure during compaction, which is beneficial for preserving intergranular pores [57]. Meanwhile, clay minerals occupy primary pores and cut pore throats, resulting in a decrease in effective porosity. Therefore, sandstone with a coarser grain size is more likely to develop bigger total porosity and effective porosity compared with finer-grained sandstone [26]. In the testing sandstone samples, the finer the grain sizes, the less the pore space. The coarser the grain size, the larger the pore space [55]. The coarser the grains, the larger the effective porosity and the larger the permeability. This suggests that the effective porosity of sandstone has a positive correlation with the permeability value. Therefore, the effective porosity of sandstone is a sensitive indicator for evaluating the permeability of the tight sandstone reservoirs.

The effective porosity has a dominant effect on the S_s, and S_s is negatively correlated with the effective porosity. S_s of HJD1-01 was only about 0.27–0.42 times that of the other samples when the effective porosity of HJD1-01 was 2.6–3 times that of other sandstone samples. It can be seen from HJD1-10 and HJD1-06 that S_s is not only affected by the effective porosity, but also by the total porosity. The effective porosity of HJD1-06 and HJD1-10 was 0.60 and 0.51, which appears closer. S_s increases as the effective stress gradually increases. However, in a certain stress scope, the S_s of the fine sandstone (HJD-06) with higher effective porosity may be bigger than that of the siltstone (HJD-10) with lower effective porosity. It is speculated that the total porosity of sandstone also has a certain influence on S_s due to the total porosity of HJD-10 being a bit bigger than that of HJD-06.

Another reason for the increase of S_s of fine sandstone and siltstone compared to medium sandstone may be the content of plastic minerals. Clay minerals tend to increase with the decrease of sandstone grain size. The content and type of plastic minerals are one factor that determines the difference in S_s; that is, the higher the content of plastic minerals such as mica and clay, the stronger the S_s of the tight rock reservoir.

6. Conclusions

An experimental study was conducted to investigate the pore characteristics and permeability in coal-measure sandstones based on the pulse attenuation gas permeability tester and LF-NMR. The permeability variation with the effective stress and grains and the effects of NMR pore characteristics on permeability variation were analyzed in detail. The following conclusions were obtained:

(1) Although the micropores are the most developed in sandstones from coal-measure, most of the micropores are the immovable pores. The pore characteristics are significantly affected by the grain size of sandstones in coal-measure. The movable pores and effective porosity increase with the grain size of testing sandstones. The pore connectivity ranks from good to poor with decreasing sandstone particle size.

(2) The relationship between the permeability and the effective stress is close to the linear relationship as the effective stress is between 405 psi and 808 psi. The greater the number of movable pores and the effective porosity, the bigger the permeability of the sandstone. The effective porosity of sandstone is a sensitive indicator for evaluating the permeability of tight sandstone reservoirs. S_s would increase for the same sample with the increase of the effective stress, whilst the effective porosity is negatively correlated with S_s. The particle size of sandstone from coal-measure has a great influence on permeability and S_s. Under similar stress conditions, the permeability of the sampling sandstones increases with the increase of the grain size. The sandstone with lower permeability and finer grains has a higher S_s.

Author Contributions: H.H. wrote the paper, conducted the experimental study, analyzed the results; Y.S. and X.C. wrote the paper, contributed to processing the raw data and completing the figures; Z.W., M.L. and S.Q. edited the original draft and made the tables. All authors have read and agreed to the published version of the manuscript.

Funding: This research was supported by the Fundamental Research Funds for the Central Universities (2019XKQYMS57), a project funded by the Priority Academic Program Development of Jiangsu Higher Education Institutions in China, Mining fissure field characteristics in high gas working panels in Jixi mining area and its influence on gas control (No. 2021060117), Influence of geological tectonic evolution on gas occurrence and migration in Xishan mining area, and the geological survey project of the China Geological Survey (No. DD20190101).

Informed Consent Statement: Not applicable.

Data Availability Statement: Not applicable.

Conflicts of Interest: The authors declare no conflict of interest.

References

1. Hou, X.W.; Zhu, Y.M.; Chen, S.B.; Wang, Y.; Liu, Y. Investigation on pore structure and multifractal of tight sandstone reservoirs in coal bearing strata using LF-NMR measurements. *J. Pet. Sci. Eng.* **2020**, *187*, 13. [CrossRef]
2. Su, X.B.; Li, F.; Su, L.A.; Wang, Q. The experimental study on integrated hydraulic fracturing of coal measures gas reservoirs. *Fuel* **2020**, *270*, 7. [CrossRef]
3. Law, B.E.; Curtis, J.B. Introduction to unconventional petroleum systems. *AAPG Bull.* **2002**, *86*, 1851–1852.
4. Sun, W.; Zuo, Y.; Wu, Z.; Liu, H.; Xi, S.; Shui, Y.; Wang, J.; Liu, R.; Lin, J. Fractal analysis of pores and the pore structure of the Lower Cambrian Niutitang shale in northern Guizhou province: Investigations using NMR, SEM and image analyses. *Mar. Pet. Geol.* **2019**, *99*, 416–428. [CrossRef]
5. Wan, L.M.; Hou, B.; Tan, P.; Chang, Z.; Muhadasi, Y. Observing the effects of transition zone properties on fracture vertical propagation behavior for coal measure strata. *J. Struct. Geol.* **2019**, *126*, 69–82. [CrossRef]
6. Hou, X.W.; Zhu, Y.M.; Yao, H.P. Coupled accumulation characteristics of Carboniferous-Permian coal measure gases in the Northern Ordos Basin, China. *Arab. J. Geosci.* **2018**, *11*, 13. [CrossRef]
7. Jiao, P.F.; Wang, P.W.; Zhou, S.W.; Wang, H.C.; Chen, X.Y. Study on the Microscopic Pore Structures of Coal Measure Reservoirs in the Shanxi Formation, Eastern Ordos Basin. *Front. Earth Sci.* **2022**, *10*, 903588. [CrossRef]
8. Jia, J.; Cao, L.; Sang, S.; Yi, T.; Zhou, X. A case study on the effective stimulation techniques practiced in the superposed gas reservoirs of coal-bearing series with multiple thin coal seams in Guizhou, China. *J. Pet. Sci. Eng.* **2016**, *146*, 489–504. [CrossRef]
9. Towler, B.; Firouzi, M.; Underschultz, J.; Rifkin, W.; Garnett, A.; Schultz, H.; Esterle, J.; Tyson, S.; Witt, K. An overview of the coal seam gas developments in Queensland. *J. Nat. Gas Sci. Eng.* **2016**, *31*, 249–271. [CrossRef]
10. Gao, H.; Li, H.A. Pore structure characterization, permeability evaluation and enhanced gas recovery techniques of tight gas sandstones. *J. Nat. Gas Sci. Eng.* **2016**, *28*, 536–547. [CrossRef]
11. Qin, Y. Research progress of symbiotic accumulation of coal measure gas in China. *Nat. Gas Ind. B* **2018**, *5*, 466–474. [CrossRef]
12. Mehmani, A.; Mehmani, Y.; Prodanovi, M.; Balhoff, M. A forward analysis on the applicability of tracer breakthrough profiles in revealing the pore structure of tight gas sandstone and carbonate rocks. *Water Resour. Res.* **2015**, *51*, 4751–4767. [CrossRef]
13. Liu, M.; Xie, R.; Guo, J.; Jin, G. Characterization of Pore Structures of Tight Sandstone Reservoirs by Multifractal Analysis of the NMR T 2 Distribution. *Energy Fuels* **2018**, *32*, 12218–12230. [CrossRef]
14. Yao, Y.B.; Liu, D.M.; Che, Y.; Tang, D.Z.; Tang, S.H.; Huang, W.H. Petrophysical characterization of coals by low-field nuclear magnetic resonance (NMR). *Fuel* **2010**, *89*, 1371–1380. [CrossRef]
15. Hou, X.; Zhu, Y.; Wang, Y.; Liu, Y. Experimental study of the interplay between pore system and permeability using pore compressibility for high rank coal reservoirs. *Fuel* **2019**, *254*, 115712. [CrossRef]
16. Kong, X.; Xiao, D.; Jiang, S.; Lu, S.; Sun, B.; Wang, J. Application of the combination of high-pressure mercury injection and nuclear magnetic resonance to the classification and evaluation of tight sandstone reservoirs: A case study of the Linxing Block in the Ordos Basin. *Nat. Gas Ind. B* **2020**, *7*, 433–442. [CrossRef]
17. Yao, Y.; Liu, D. Comparison of low-field NMR and mercury intrusion porosimetry in characterizing pore size distributions of coals. *Fuel* **2012**, *95*, 152–158. [CrossRef]
18. Xiao, D.; Lu, Z.; Jiang, S.; Lu, S. Comparison and integration of experimental methods to characterize the full-range pore features of tight gas sandstone-A case study in Songliao Basin of China. *J. Nat. Gas Sci. Eng.* **2016**, *34*, 1412–1421. [CrossRef]
19. Hinai, A.A.; Rezaee, R.; Esteban, L.; Labani, M. Comparisons of pore size distribution: A case from the Western Australian gas shale formations. *J. Unconv. Oil Gas Resour.* **2014**, *8*, 1–13. [CrossRef]
20. Li, M.; Wang, D.; Shao, Z. Experimental study on changes of pore structure and mechanical properties of sandstone after high-temperature treatment using nuclear magnetic resonance. *Eng. Geol.* **2020**, *275*, 105739. [CrossRef]
21. Yao, Y.; Liu, D.; Liu, J.; Xie, S. Assessing the Water Migration and Permeability of Large Intact Bituminous and Anthracite Coals Using NMR Relaxation Spectrometry. *Transp. Porous Media* **2015**, *107*, 527–542. [CrossRef]

22. Cai, Y.; Liu, D.; Pan, Z.; Yao, Y.; Li, J.; Qiu, Y. Petrophysical characterization of Chinese coal cores with heat treatment by nuclear magnetic resonance. *Fuel* **2013**, *108*, 292–302. [CrossRef]
23. Kleinberg, R.L.; Straley, C.; Kenyon, W.E.; Akkurt, R.; Farooqui, S.A. Nuclear Magnetic Resonance of Rocks: T1 vs. T2. In Proceedings of the SPE Annual Technical Conference and Exhibition, Houston, TX, USA, 3 October 1993.
24. Qu, Y.; Sun, W.; Tao, R.; Luo, B.; Chen, L.; Ren, D. Pore–throat structure and fractal characteristics of tight sandstones in Yanchang Formation, Ordos Basin. *Mar. Pet. Geol.* **2020**, *120*, 104573. [CrossRef]
25. Huang, W.; Lu, S.; Hersi, O.S.; Wang, M.; Deng, S.; Lu, R. Reservoir spaces in tight sandstones: Classification, fractal characters, and heterogeneity. *J. Nat. Gas Sci. Eng.* **2017**, *46*, 80–92. [CrossRef]
26. Zhang, N.; He, M.C.; Zhang, B.; Qiao, F.C.; Sheng, H.L.; Hu, Q.H. Pore structure characteristics and permeability of deep sedimentary rocks determined by mercury intrusion porosimetry. *J. Earth Sci.* **2016**, *27*, 670–676. [CrossRef]
27. Moosavi, S.A.; Goshtasbi, K.; Kazemzadeh, E.; Bakhtiari, H.A.; Esfahani, M.R.; Vali, J. Relationship between porosity and permeability with stress using pore volume compressibility characteristic of reservoir rocks. *Arab. J. Geosci.* **2014**, *7*, 231–239. [CrossRef]
28. Shao, X.H.; Pang, X.Q.; Jiang, F.J.; Li, L.L.; Huyan, Y.Y.; Zhene, D.Y. Reservoir Characterization of Tight Sandstones Using Nuclear Magnetic Resonance and Incremental Pressure Mercury Injection Experiments: Implication for Tight Sand Gas Reservoir Quality. *Energy Fuels* **2017**, *31*, 10420–10431. [CrossRef]
29. Li, Y.; Tang, D.Z.; Xu, H.; Meng, Y.J.; Li, J.Q. Experimental research on coal permeability: The roles of effective stress and gas slippage. *J. Nat. Gas Sci. Eng.* **2014**, *21*, 481–488. [CrossRef]
30. Ma, Q.; Harpalani, S.; Liu, S. A simplified permeability model for coalbed methane reservoirs based on matchstick strain and constant volume theory. *Int. J. Coal Geol.* **2011**, *85*, 43–48. [CrossRef]
31. Wu, S.; Tang, D.Z.; Li, S.; Wu, H.Y.; Hu, X.; Zhu, X.G. Effects of geological pressure and temperature on permeability behaviors of middle-low volatile bituminous coals in eastern Ordos Basin, China. *J. Pet. Sci. Eng.* **2017**, *153*, 372–384. [CrossRef]
32. Khormali, A.; Bahlakeh, G.; Struchkov, I.; Kazemzadeh, Y. Increasing inhibition performance of simultaneous precipitation of calcium and strontium sulfate scales using a new inhibitor—Laboratory and field application. *J. Pet. Sci. Eng.* **2021**, *202*, 108589. [CrossRef]
33. Li, X.; Fu, X.H.; Ranjith, P.G.; Xu, J. Stress sensitivity of medium- and high volatile bituminous coal: An experimental study based on nuclear magnetic resonance and permeability-porosity tests. *J. Pet. Sci. Eng.* **2019**, *172*, 889–910. [CrossRef]
34. Tao, S.; Wang, Y.; Tang, D.; Xu, H.; Lv, Y.; He, W.; Li, Y. Dynamic variation effects of coal permeability during the coalbed methane development process in the Qinshui Basin, China. *Int. J. Coal Geol.* **2012**, *93*, 16–22. [CrossRef]
35. Li, S.; Tang, D.Z.; Pan, Z.J.; Xu, H.; Huang, W.Q. Characterization of the stress sensitivity of pores for different rank coals by nuclear magnetic resonance. *Fuel* **2013**, *111*, 746–754. [CrossRef]
36. Shen, J.; Qin, Y.; Li, Y.P.; Yang, Y.H.; Ju, W.; Yang, C.L.; Wang, G. In situ stress field in the FZ Block of Qinshui Basin, China: Implications for the permeability and coalbed methane production. *J. Pet. Sci. Eng.* **2018**, *170*, 744–754. [CrossRef]
37. Meng, Y.F.; Luo, C.B.; Li, G.; Liu, H.B. An experimental study on stress sensitivity of tight sandstone gas reservoirs during nitrogen drilling. *Arab. J. Geosci.* **2019**, *12*, 11. [CrossRef]
38. Zhang, H.; Zhong, Y.; Kuru, E.G.; Kuang, J.C.; Sh, J.P. Impacts of permeability stress sensitivity and aqueous phase trapping on the tight sandstone gas well productivity—A case study of the Daniudi gas field. *J. Pet. Sci. Eng.* **2019**, *177*, 261–269. [CrossRef]
39. Zhang, K.; Sang, S.X.; Liu, C.J.; Ma, M.Y.; Zhou, X.Z. Experimental study the influences of geochemical reaction on coal structure during the CO_2 geological storage in deep coal seam. *J. Pet. Sci. Eng.* **2019**, *178*, 1006–1017. [CrossRef]
40. Li, S.J.; Wang, Z.H.; Sun, Y.X.; Xie, J.B. Stress Sensitivity of Low-permeability Sandstone Reservoir. In *Materials Processing and Manufacturing III, Pts 1–4*; Advanced Materials Research; Sang, X., Kim, Y.H., Eds.; Trans Tech Publications Ltd.: Durnten-Zurich, Switzerland, 2013; Volume 753–755, pp. 686–689.
41. Archer, R. Impact of Stress Sensitive Permeability on Production Data Analysis. In Proceedings of the SPE Unconventional Reservoirs Conference, Keystone, CO, USA, 10–12 February 2008. [CrossRef]
42. Fatt, I.; Davis, D.H. Reduction in Permeability with Overburden Pressure. *J. Pet. Technol.* **1952**, *4*, 16. [CrossRef]
43. Liu, J.-Q.; Zhang, C.-M.; Zhang, Z. Combine the capillary pressure curve data with the porosity to improve the prediction precision of permeability of sandstone reservoir. *J. Pet. Sci. Eng.* **2016**, *139*, 43–48. [CrossRef]
44. Davies, J.P.; Davies, D.K. Stress-Dependent Permeability: Characterization and Modeling. *Spe J.* **2001**, *6*, 224–235. [CrossRef]
45. Volokitin, Y.; Looyestijn, W.J.; Sli, J.; Kerman, W.; Hofman, J.P. A practical approach to obtain primary drainage capillary pressure curves from NMR core and log data. *Petrophysics* **2001**, *42*, 334–343.
46. Ghomeshi, S.; Kryuchkov, S.; Kantzas, A. An investigation into the effects of pore cconnectivity on T2 NMR relaxation. *J. Magn. Reson.* **2018**, *289*, 79–91. [CrossRef] [PubMed]
47. Zhang, Z.; Qin, Y.; Zhuang, X.; Li, G.; Wang, X. Poroperm characteristics of high-rank coals from Southern Qinshui Basin by mercury intrusion, SEM-EDS, nuclear magnetic resonance and relative permeability analysis. *J. Nat. Gas Sci. Eng.* **2018**, *51*, 116–128. [CrossRef]
48. Straley, C.; Rossini, D.; Vinegar, H.J.; Tutunjian, P.N.; Morriss, C.E. Core analysis by low-field NMR. *Log. Anal.* **1997**, *38*, 84–93.
49. Al-Mahrooqi, S.H.; Grattoni, C.A.; Moss, A.K.; Jing, X.D. An investigation of the effect of wettability on NMR characteristics of sandstone rock and fluid systems. *J. Pet. Sci. Eng.* **2003**, *39*, 389–398. [CrossRef]

50. Lai, J.; Wang, G.; Cao, J.; Xiao, C.; Wang, S.; Pang, X.; Dai, Q.; He, Z.; Fan, X.; Yang, L.; et al. Investigation of pore structure and petrophysical property in tight sandstones. *Mar. Pet. Geol.* **2018**, *91*, 179–189. [CrossRef]
51. Song, Z.Y.; Ji, H.G.; You, S.; Tan, J.; Wang, H. Experimental Study on Sensitivity to Temperature Stress of the Permeability of Weakly Cemented Sandstone. In Proceedings of the 3rd International Conference on Advances in Energy Resources and Environment Engineering, Harbin, China, 8–10 December 2017; IOP Conference Series-Earth and Environmental Science. IOP Publishing Ltd.: Bristol, UK, 2018; Volume 113.
52. Mclatchie, A.S.; Hemstock, R.A.; Young, J.W. The Effective Compressibility of Reservoir Rock and Its Effects on Permeability. *J. Pet. Technol.* **1958**, *10*, 49–51. [CrossRef]
53. Vairogs, J.; Hearn, C.L.; Dareing, D.W.; Rhoades, V.W. Effect of Rock Stress on Gas Production From Low-Permeability Reservoirs. *J. Pet. Technol.* **1971**, *23*, 1161–1167. [CrossRef]
54. Yin, S.; Dong, L.; Yang, X.; Wang, R. Experimental investigation of the petrophysical properties, minerals, elements and pore structures in tight sandstones. *J. Nat. Gas Sci. Eng.* **2020**, *76*, 103189. [CrossRef]
55. Li, Z.; Wu, S.; Xia, D.; He, S.; Zhang, X. An investigation into pore structure and petrophysical property in tight sandstones: A case of the Yanchang Formation in the southern Ordos Basin, China. *Mar. Pet. Geol.* **2018**, *97*, 390–406. [CrossRef]
56. Zhao, H.; Ning, Z.; Zhao, T.; Zhang, R.; Wang, Q. Effects of mineralogy on petrophysical properties and permeability estimation of the Upper Triassic Yanchang tight oil sandstones in Ordos Basin, Northern China. *Fuel* **2016**, *186*, 328–338. [CrossRef]
57. Zhong, D.; Zhou, L.; Sun, H. Influences of petrologic features on diagenesis and pore development: An example from the Triassic Yanchang Formation in Longdong Area, Ordos Basin. *Oil Gas Geol.* **2012**, *33*, 280–289.